ACS OMEGA

http://pubs.acs.org/journal/acsodf

Article

Label-Free, Highly Sensitive Electrochemical Aptasensors Using Polymer-Modified Reduced Graphene Oxide for Cardiac Biomarker Detection

Abhinav Sharma,[‖] Jyoti Bhardwaj,[‖] and Jaesung Jang*

Cite This: *ACS Omega* 2020, 5, 3924−3931

Read Online

ACCESS | Metrics & More | Article Recommendations | Supporting Information

ABSTRACT: Acute myocardial infarction (AMI), also recognized as a "heart attack," is one leading cause of death globally, and cardiac myoglobin (cMb), an important cardiac biomarker, is used for the early assessment of AMI. This paper presents an ultrasensitive, label-free electrochemical aptamer-based sensor (aptasensor) for cMb detection using polyethylenimine (PEI)-functionalized reduced graphene oxide (PEI−rGO) thin films. PEI, a cationic polymer, was used as a reducing agent for graphene oxide (GO), providing highly positive charges on the rGO surface and allowing direct immobilization of negatively charged single-strand DNA aptamers against cMb via electrostatic interaction without any linker or coupling chemistry. The presence of cMb was detected on Mb aptamer-modified electrodes using differential pulse voltammetry via measuring the current change due to the direct electron transfer between the electrodes and cMb proteins (Fe^{3+}/Fe^{2+}). The limits of detection were 0.97 pg mL^{-1} (phosphate-buffered saline) and 2.1 pg mL^{-1} (10-fold-diluted human serum), with a linear behavior with logarithmic cMb concentration. The specificity and reproducibility of the aptasensors were also examined. This electrochemical aptasensor using polymer-modified rGO shows potential for the early assessment of cMb in point-of-care testing applications.

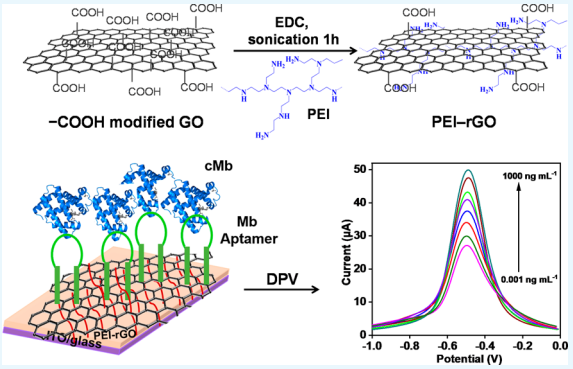

1. INTRODUCTION

Acute myocardial infarction (AMI) is one of the fatal diseases for humans. Although electrocardiography is extensively used for early detection of AMI, only 57% of AMI patients are accurately diagnosed, with some showing normal ECG or nondiagnostic results when diagnosed by an emergency department.[1,2] Therefore, the measurement of cardiac biomarkers in a blood sample is a useful and essential diagnostic tool for AMI, and the biomarkers include cardiac myoglobin (cMb) and cardiac troponins I and T. Cardiac troponins are considered the most specific biomarkers for AMI diagnosis but not used as early detection biomarkers for AMI.[3] In contrast, cMb is a biomarker for early detection of AMI because of its quick release into the blood from damaged cardiac muscles than any others after the onset of AMI.[4] cMb concentration in the blood increases rapidly within 1−3 h and reaches the peak within 6−12 h.[4] In human serum, cMb concentration is considered normal in a range of 30−90 ng mL^{-1} and increases up to approximately 200 ng mL^{-1} within 6−12 h after AMI.[5]

To date, several methods have been used for cMb detection such as enzyme-linked immunosorbent assay;[5] mass spectrometry;[6] liquid chromatography;[7] surface plasmon resonance;[8,9] colorimetric,[10] fluorescence,[11] and polyaniline nanowire biosensors;[12] molecularly imprinted polymer (MIP) sensors;[13] and MIP-based electrochemical sensors.[14,15] Among the reported methods, the MIP technique provides synthetic recognition materials for biomarkers, which can increase the robustness of the device.[15] However, despite their advances, MIP-based sensors have several chemical problems in cross-linking, which leads to the polymer layers with different binding sites and differences between the batches of preparation.[16] In comparison with antibodies and MIPs, aptamers are short nucleic acids with loop-like secondary structures, enabling their binding with target molecules with good affinity and specificity.[17] Furthermore, aptamers possess several advantages such as low cost, high reproducibility, and thermal stability, and it can be modified easily with several functional groups.[18] Moreover, the electrochemical technique is especially favorable for cMb detection as myoglobin (Fe^{3+}/Fe^{2+}) is redox-active, which allows the direct electron transfer between the electrode and the protein,[19] possessing advantages such as high sensitivity, simple instrumentation, rapid analysis, and low cost.[18,20]

Received: October 10, 2019
Accepted: February 5, 2020
Published: February 18, 2020

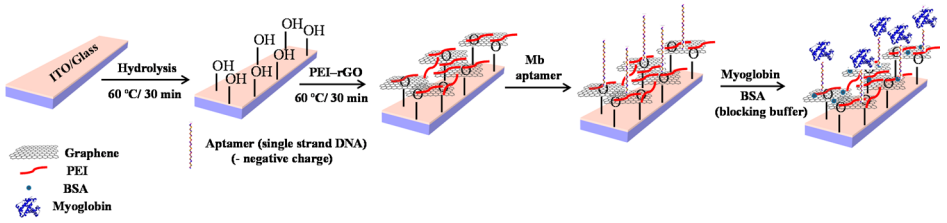

Figure 1. Schematic of the functionalization process of the PEI−rGO aptasensor.

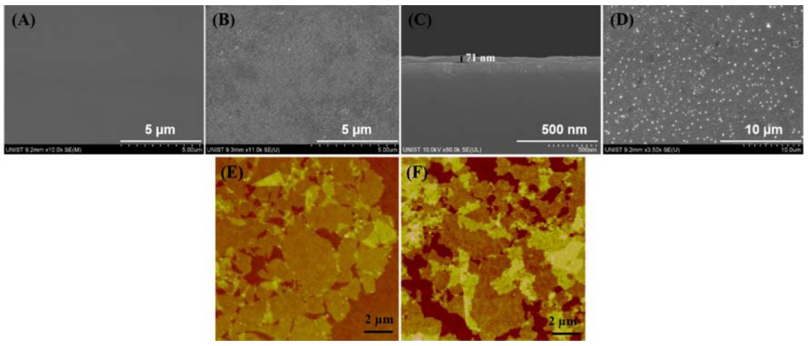

Figure 2. FE-SEM images of the (A) bare ITO/glass electrode and (B) PEI−rGO film coated onto the ITO/glass electrode and (C) cross section of the layered thin film of PEI−rGO and (D) cMb aptamers (10 μg mL^{-1}) immobilized onto the PEI−rGO film. AFM images of the (E) GO sheets and (F) PEI−rGO sheets.

Until date, graphene or reduced graphene oxide (rGO) has been explored to improve the performance of electrochemical biosensors,[21] owing to its most attractive mechanical and electrical properties.[22,23] Numerous chemicals such as hydrazine,[24] dimethylhydrazine,[25] and $NaBH_4$[26] are used for reduction of graphene oxide (GO) to rGO, and they are mostly toxic or explosive. Irreversible aggregates of rGO sheets also form during the reduction process through van der Waals forces, making it difficult to have dispersity and stability in water. Hence, various polymers such as polyaniline,[27] polypyrrole,[28] polyallylamine,[29] poly(vinyl alcohol),[30] and poly(diallyl dimethylammonium chloride)[31] have been used for the modification to improve their electrical and optical properties in electrochemical biosensing. Moreover, rGO functionalized with hydrophilic polymers can prevent aggregation in aqueous media and reduce GO to rGO simultaneously.

Polyethylenimine (PEI) is a hydrophilic, cationic polymer with a high density of amine ($+NH_2$) groups, which provides positive charges on the surface. Because of its active amine groups, PEI can easily attach to certain active groups of GO (e.g., carboxyl or epoxy groups) covalently and simultaneously reduce GO to PEI−rGO, minimizing the synthesis steps and increasing the conductivity. Moreover, PEI can act as an electron promoter between the electrode and electrolyte solution, leading to a more sensitive response; hence, it can be a perfect candidate for the surface modification of GO and electrochemical sensors.[32,33] However, only a few reports on PEI-graphene-based electrochemical biosensors have been presented for detection of the following analytes: H_2O_2,[34,35] dopamine,[36,37] *Escherichia coli*,[38] glucose,[39] gallic acid,[40] metal ions,[41] and gas molecules.[42] Furthermore, the applications and schemes of PEI−rGO in these studies are completely or quite different from those of the present study. For example, previously PEI-functionalized GO was used as a vector for gene delivery,[33] used for immobilizing a model enzyme, CYP2D6,[43] or used for detecting cardiac troponins using the electrophoretic deposition method.[44]

In this study, we demonstrate an ultrasensitive and label-free electrochemical aptamer-based sensor (aptasensor) for cMb detection using PEI-grafted rGO thin films. A simple chemical route was used for the synthesis of the PEI−rGO matrix with improved electronic properties for electrochemical biosensors at room temperature. In brief, GO was synthesized using the modified Hummer's method,[45] and PEI was grafted onto the GO surface, allowing positive charges onto the GO surface and reducing it to rGO. The synthesized PEI−rGO was deposited as a thin and uniform film with a wide range of thicknesses (from nm to μm) using the drop-casting method,[46] which has various advantages over other deposition techniques such as simple, cost-effective, fast, and room-temperature method. The film thickness can be controlled by tuning a few parameters such as volume, concentration of the solution, and so forth. The PEI−rGO thin film provided large, positively charged surfaces, which is critical in adsorbing the negatively charged cMb aptamers without any linker or coupling chemistry.[47] Moreover, PEI−rGO could accelerate electron transfer, enabling signal amplification without the use of enzymes or nanoparticles. This proposed electrochemical aptasensor shows numerous advantages over conventional approaches such as enhanced limit of detection (LOD), wide linear ranges, sensitivity, reusability, and reproducibility.

2. RESULTS AND DISCUSSION

2.1. Characterization of PEI−rGO-Coated ITO/Glass Electrodes. Figure 1 represents the functionalization process of the PEI−rGO aptasensor. Field-emission scanning electron microscopy (FE-SEM) images of a bare ITO/glass (Figure 2A) and PEI−rGO thin film-coated ITO/glass electrode (Figure 2B) showed a uniform and thin film covering a large surface area on the electrode. Figure 2C shows the cross section of the layered thin film of PEI−rGO, demonstrating that a highly

https://dx.doi.org/10.1021/acsomega.9b03368
ACS Omega 2020, 5, 3924−3931

ordered thin film can be deposited by drop-casting via controlling the concentration and volume of the solution. Moreover, the coffee-ring effect was negligible in this study because of strong interactions between the PEI-rGO sheets and the hydrolyzed ITO substrates.[46] An FE-SEM image of an Mb aptamer-modified PEI−rGO surface showed many tiny and bright clusters on the surfaces, implying the immobilization of Mb aptamers (Figure 2D). The atomic force microscopy (AFM) images of the GO sheets (Figure 2E) and PEI−rGO sheets (Figure 2F) showed homogenous dispersion on the surface. The high-resolution transmission electron microscopy (HR-TEM) images of GO and PEI−rGO showed the opaque and sheet-like structure on a carbon copper grid (Figure S2A) and transparent and thin layers of rGO after reduction by PEI (Figure S2B), respectively.

The UV−vis spectra (Figure S3) and the Raman spectra (Figure S4) of both the GO and PEI−rGO matrix showed successful reduction of GO upon functionalization with PEI or the formation of PEI−rGO. The polymer reduction was also characterized by X-ray photoelectron spectroscopy (XPS) analysis, which is considered a useful tool to identify the removal and evolution of functional groups.[48,49] The XPS spectra of GO and PEI−rGO thin films showed both peaks of C 1s and O 1s at 284.6 and 530 eV, respectively (Figure 3A).

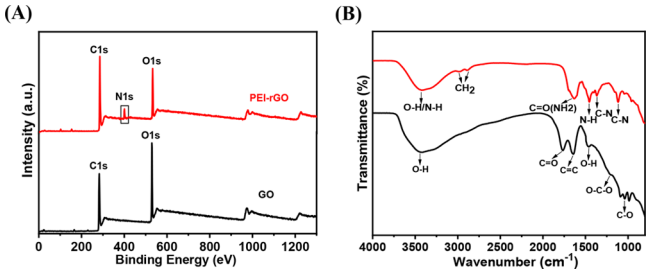

Figure 3. Structural characterization of the GO and PEI−rGO thin film for analyses of surface modification and reduction of GO by PEI with various spectroscopic techniques: (A) XPS and (B) FTIR spectra of GO and PEI−rGO thin films.

In the XPS spectra of GO, the oxygen peak intensity was stronger than that of the carbon. However, in the XPS spectra of the PEI−rGO thin film, the carbon peak was stronger than the oxygen peak owing to the reduction, which evidently shows that oxygen-containing groups for PEI−rGO were significantly eliminated. The additional new peak N 1s at 398 eV was observed, indicating a high density of $-NH_2$ groups of PEI chains introduced onto the GO surface and hence reduction to PEI−rGO. The C 1s XPS spectra of GO and PEI-rGO are shown in Figure S5A,B.

The Fourier transform infrared spectroscopy−attenuated total reflectance (FTIR−ATR) spectra of GO showed stretching vibrations for functional groups such as O−H (3400 cm^{-1}), C═O (1735 cm^{-1}), C═C (1633 cm^{-1}), C−O (1050 cm^{-1}), and C−O−C (1217 cm^{-1}) (Figure 3B).[50,51] In addition, the bending vibration peak of the O−H group was measured at 1423 cm^{-1}. For the PEI−rGO spectra, the stretching vibration of $-NH_2$/NH groups was found at 3400 cm^{-1} and an absorption doublet peak at 2851 and 2924 cm^{-1} was observed, which was attributed to the $-CH_2$ symmetric and antisymmetric stretching vibration of the PEI chain.[52] After reduction, the stretching frequency (1735 cm^{-1}) to C═O was shifted to 1630 cm^{-1} owing to the CO−NH bond formation.[53] The new peaks appeared at 1455 cm^{-1} for bending vibration of the N−H group and at 1363 and 1108 cm^{-1} because of the C−N stretching vibration. These FTIR results indicate the successful incorporation of PEI into −COOH-modified GO.[52]

2.2. Electrochemical Studies of Modified ITO/Glass Electrodes. Figure 4A shows the cyclic voltammetry (CV) measurements of the electrodes with different functionalizations (ITO/glass, GO/ITO/glass, PEI/ITO/glass, PEI−rGO/ITO/glass, Mb-apta/PEI−rGO/ITO/glass, and BSA/Mb-apta/PEI−rGO/ITO/glass). The peak current for a GO/ITO/glass electrode (149 μA) was less than that of a bare ITO/glass electrode (207 μA), which might be due to a reduction in electron transfer caused by a GO layer. The peak current for PEI−rGO/ITO/glass increased up to 287 μA after modification with PEI−rGO in comparison with those of PEI/ITO/glass (254 μA) and GO/ITO/glass (149 μA) owing to the high electron transfer property of PEI−rGO. The insulating behavior and entrapment of redox active sites by aptamers blocked the electron transfer and hence decreased the peak current to 52.3 μA after immobilization of Mb aptamers. We observed that the peak current was further decreased to 41.2 μA after bovine serum albumin (BSA) binding because of the insulating behavior of the BSA protein. The differential pulse voltammetry (DPV) measurements (Figure 4B) agreed well with the CV ones.

The interfacial changes induced during the immobilization were also recorded by electrochemical impedance spectroscopy (EIS) (Figure 4C) at an electric potential of 0.1 V and an amplitude of 10 mV in a frequency range (0.1 Hz to 100 kHz).

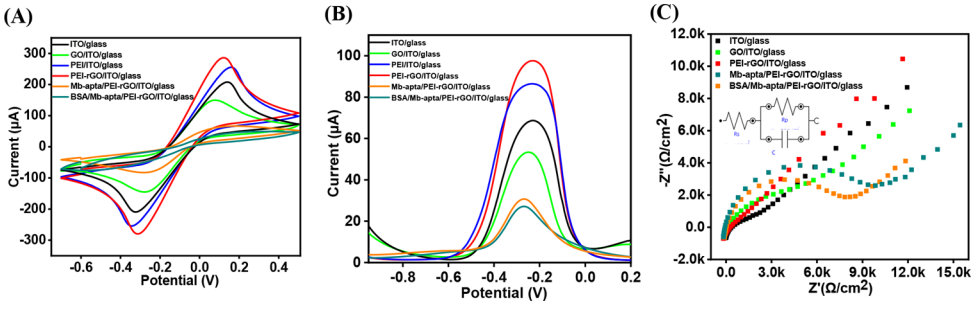

Figure 4. (A) Cyclic voltammograms and (B) differential pulse voltammograms of ITO/glass, GO/ITO/glass, PEI/ITO/glass, PEI−rGO/ITO/glass, Mb-apta/PEI-rGO/ITO/glass, and BSA/Mb-apta/PEI-rGO/ITO/glass-modified electrodes. (C) EIS spectra of ITO/glass, GO/ITO/glass, PEI−rGO/ITO/glass, Mb-apta/PEI-rGO/ITO/glass, and BSA/Mb-apta/PEI-rGO/ITO/glass-modified electrodes in PBS buffer with 5 mM $K_3[Fe(CN)_6]/K_4[Fe(CN)_6]$ and 0.5 M KCl.

https://dx.doi.org/10.1021/acsomega.9b03368
ACS Omega 2020, 5, 3924−3931

The charge transfer resistance (R_{CT}), solution resistance (R_S), and double-layer capacitance (C_{dl}) were computed during the different stages of our electrochemical aptasensor development (Table S1). The R_{CT} (1.9 kΩ) for the ITO/glass electrode increased up to 3.7 kΩ after GO deposition and was decreased (710 Ω) after deposition of PEI−rGO/ITO/glass. This was due to the cross-linking of sheets with one another in the existence of PEI, which increased the electron transfer rate.[54] The R_{CT} value increased to 6.8 kΩ after aptamer immobilization, which indicates the binding of aptamers on the PEI−rGO-modified electrode surface owing to the interaction between PEI (positive charges) and aptamers (negative charges). A further increase in the R_{CT} value (9.31 kΩ) for a BSA/Mb-apta/PEI−rGO/ITO/glass electrode was measured after BSA deposition, which covered the nonspecific sites of the Mb-apta/PEI−rGO/ITO electrode and blocked the electron transfer. Scan rate studies were conducted for the BSA/Mb-apta/PEI−rGO/ITO/glass electrode with varying scan rates (10−120 mV/s) (Figure S6).

2.3. Optimization of Aptamer Concentration and Response Time. DPV was used to determine the optimal concentration of the aptamer bound to the PEI−rGO/ITO/glass electrode. The electrode current decreased with the increasing Mb aptamer (Mb-apta) concentrations (2−20 μg mL^{-1}) and was saturated at a concentration of 12 μg mL^{-1} (Figure S7A). The peak current of the BSA/Mb-apta/PEI−rGO/ITO/glass electrode was also measured at a cMb concentration of 100 ng mL^{-1} as the incubation time was varied from 5 to 60 min. A rapid increase in the peak current with an increase in incubation time was observed, and the current was saturated around 30 min, resulting in the maximum binding of the cMb antigens to the electrode surface (Figure S7B).

2.4. Electrochemical Detection of cMb. DPV was conducted to determine the electrochemical response of the BSA/Mb-apta/PEI−rGO/ITO/glass electrode for various cMb concentrations (0.001−1000 ng mL^{-1}) in phosphate-buffered saline (PBS; pH 7.4, 1×) (Figure 5A). The peak current increased with increasing cMb concentration.[5,18,55] The reduction peak occurred at a potential of −0.5 V for all cMb concentrations owing to the reduction of the Fe moiety present in cMb. Moreover, reduction of Fe^{3+} to Fe^{2+} can occur at an electrode surface by the transfer of one electron.[19] The peak current exhibited a linear relationship (R^2 = 0.98) with the logarithm of cMb concentration (0.001−1000 ng mL^{-1}) in PBS (Figure 5B). The sensitivity of the electrode and LOD based on a signal-to-noise ratio of 3 was calculated to be 3.77 μA mL ng^{-1} and 0.97 pg mL^{-1}, respectively. The PEI−rGO thin film provided a large surface area and appropriate configuration to the aptamer, thus stimulating the efficient aptamer−antigen binding and hence the sensitivity of the aptasensor.

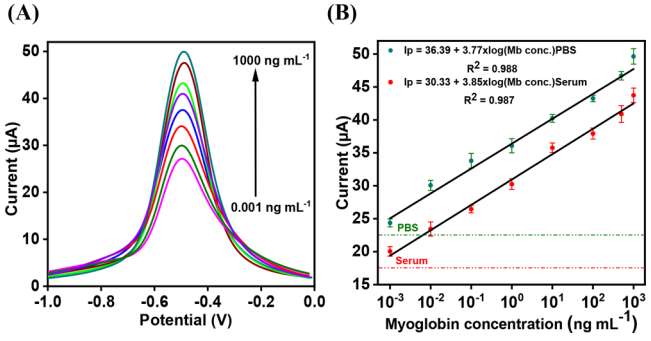

Figure 5. (A) Differential pulse voltammograms recorded in PBS for detection of cMb concentrations ranging from 0.001 to 1000 ng mL^{-1}. (B) Calibration curve for the detection of cMb concentration (0.001−1000 ng mL^{-1}) diluted in PBS and human serum (10-fold-diluted serum). The error bars represent the standard deviations of three independent measurements.

The electrochemical aptasensor was also tested for cMb concentrations (0.001−1000 ng mL^{-1}) in 10-fold-diluted human serum in PBS. A small volume (10 μL) of cMb concentrations spiked in 10-fold-diluted human serum was immobilized on the electrode (BSA/Mb-apta/PEI−rGO/ITO/glass). The peak current increased with increasing cMb concentration (Figure 5B). The aptasensor showed a linear behavior (R^2 = 0.98), and the LOD was 2.1 pg mL^{-1}. Thus, this aptasensor can be practically used for the quantitative analysis and early detection of cMb in real samples. Moreover, high electrical conductance of PEI−rGO thin films and selective binding of the aptamers enhanced the LOD and sensitivity of the aptasensor, which is comparable to other electrochemical sensors (Table 1).

2.5. Reproducibility and Stability of Aptasensors. The repeatability of the aptasensor was performed with cMb concentration (100 ng mL^{-1}) for five samples modified on the electrode (BSA/Mb-apta/PEI−rGO/ITO/glass). The response showed an acceptable relative standard deviation (RSD) of 3.8% (Table S2 & Figure 6A). To determine the stability of the aptasensors, samples (100 ng mL^{-1}) were measured on the same day and stored at two different places (4 °C and room temperature) for 15 days, and the aptasensor gained 92% after storage at 4 °C and 83% at room temperature of the initial respective current responses after 12 days (Figure 6B).

2.6. Specificity Test. To assess the specificity of the aptasensors, cardiac-specific troponins (cTnT & cTnI) and BSA protein with concentrations of 100 ng mL^{-1} were chosen, which coincides with the biological cMb level in serum samples (Figure 6C).[56−58] The aptasensors showed negligible changes in current responses after the immobilization of cTnT, cTnI, and BSA. However, when 100 ng mL^{-1} cMb was added to the aptasensors, the current showed a rapid and sharp increase. This test shows that this aptasensor possesses high selectivity to cMb.

3. CONCLUSIONS

We have presented an ultrasensitive and label-free electrochemical aptasensor using PEI rGO (PEI−rGO) to detect cMb. A cost-effective and straightforward chemical process was adopted to synthesize PEI−rGO at room temperature. Here, PEI was used as both a surface modifier and a reducing agent in reduction of GO to PEI−rGO. The electrical conductivity of PEI−rGO thin films increased in comparison with GO, showing the direct reduction of GO by PEI. PEI provided a large number of amine groups, allowing covalent bonding on the −COOH-modified GO surface via the amide bond. Moreover, positively charged PEI−rGO surfaces allowed direct immobilization of negatively charged DNA aptamers via electrostatic interaction without any linker or coupling chemistry, reducing the functionalization step of the sensor. PEI−rGO thin films showed high electrical property and provided a large surface area, resulting in label-free and highly

https://dx.doi.org/10.1021/acsomega.9b03368
ACS Omega 2020, 5, 3924−3931

Table 1. Comparison of the Performance Characteristics of Different Electrochemical Sensors for the Detection of cMb[a]

S. no.	electrode materials	detection method	specific recognition element	media	LOD	detection range	reference
1	PEI−rGO/ITO/glass	DPV	aptamer	PBS, serum	0.97 pg mL^{-1} 2.1 pg mL^{-1}	0.001−1000 ng mL^{-1}	present work
2	GQDs/SPE	EIS	antibody	PBS	0.01 ng mL^{-1}	0.01−100 ng mL^{-1}	5
3	Fe_3O_4@SiO_2/CILE	CV		PBS	0.18 mM L^{-1}	0.2−11 mM L^{-1}	61
4	Au/SPE	EIS/SWV	MIP	HEPES	2.25 μg mL^{-1}	EIS (0.852−4.26 μg mL^{-1}). SWV (1.1−2.98 μg mL^{-1})	14
5	MB-CNTs/GCE	amperometric		PBS	20 nM	0.1−3 μM	62
6	Au/RGD/GR−COOH/GCE	DPV	aptamer	PBS	26.3 ng mL^{-1}	0.0001−0.2 gL^{-1}	63
7	AuE	EIS	antibody	PBS	5.2 ng mL^{-1}	10−650 ng mL^{-1}	64
8	DApt-CS/SPGE	DPV	aptamer	PBS	27 pM (0.45 ng mL^{-1})	0.1−40 nM	18
9	GO-AuNPs/SPE	EIS	antibody	PBS/serum	0.67 ng mL^{-1}	1−1400 ng mL^{-1}	65
10	rGO/CNT/SPE	CV	aptamer	PBS	0.34 ng mL^{-1}	1−4000 ng mL^{-1}	66
11	DDAB/Au/SPE	SWV	antibody	serum	10 ng mL^{-1}	10−1780 ng mL^{-1}	67
12	AuNPs−PAMAM/GCE	stripping voltammetry	antibody	PBS	3.8 pg mL^{-1}	0.01−500 ng mL^{-1}	55
13	Pt(MPA)/ITO/glass	EIS	antibody	PBS	1.7 ng mL^{-1}	0.01−1 μg mL^{-1}	68
14	4-ATP/AuNPs/ITO/glass	EIS	antibody	PBS	5.5 ng mL^{-1}	0.02−1 μg mL^{-1}	69
15	TCPP−Gr/AuNPs/GCE	DPV	aptamer	PBS	0.0067 nM	0.020−770 nM	70
16	MWCNTs/SPE	EIS	antibody	PBS	0.08 ng mL^{-1}	0.1−90 ng mL^{-1}	71

[a]4-ATP: 4-aminothiophenol, AuE: gold electrode, AuNPs: gold nanoparticles, GR-COOH: carboxylated graphene, CILE: carbon ionic liquid electrode, CNTs: carbon nanotubes, CV: cyclic voltammetry, DApt-CS: dual-aptamer-complementary strand aptamer conjugate, DDAB: didodecyl dimethylammonium bromide, DPV: differential pulse voltammetry, EIS: electrochemical impedance spectroscopy, Fe_3O_4@SiO_2: iron oxide core and silica shell, Gr: graphene, GQDs: graphene quantum dots, GCE: glassy carbon electrode, HEPES: hydroxyethyl piperazineethanesulfonic acid, ITO: indium tin oxide, LOD: limit of detection, MB: methylene blue, MPA: 3-mercaptopropionic acid, MWCNTs: multiwalled carbon nanotubes, MIP: molecularly imprinted polymer, PAMAM: poly(amidoamine) dendrimer, PBS: phosphate-buffered saline, PEI: polyethyleneimine, Pt(MPA): 3-Mercaptopropionic acid-functionalized Pt nanoparticles, RGD: arginine-glycine-aspartic acid, rGO: reduced graphene oxide, SAM: self-assembled monolayer, SPE: screen-printed electrode, SPGE: screen-printed gold electrode, SPR: surface plasmon resonance, SWV: square wave voltammetric, and TCPP: *meso*-tetra(4-carboxyphenyl)porphyrin.

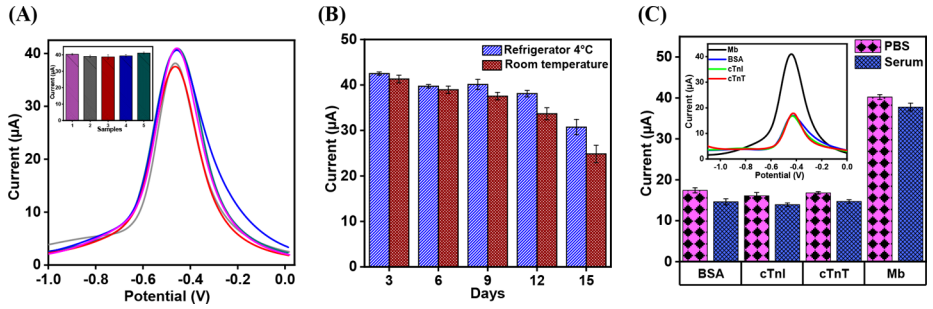

Figure 6. (A) Reproducibility of the aptasensors was evaluated using 100 ng mL^{-1} cMb concentration in five different devices. The inset represents the bar graph of five sensors. (B) Stability of the aptasensors at 4 °C and room temperature (25 °C). The current responses of the electrodes were observed at three day intervals for 15 days. (C) Selectivity of the aptasensors was evaluated against BSA, cTnI, and cTnT (100 ng mL^{-1}). The error bars represent the standard deviations of three independent measurements.

sensitive detection of cMb. It also exhibited excellent dispersibility and stability in water, allowing synthesis of homogenous and thin films. The fabricated BSA/Mb-apta/PEI−rGO/ITO electrode showed good sensitivity (3.7 μA mL ng^{-1}) with a log-linear detection range (0.001−1000 ng mL^{-1}) and notable LOD (0.97 pg mL^{-1}). The measurement of these aptasensors was ∼94% at 4 °C storage and ∼92% at room temperature storage after 15 days. Compared to other biosensors based on antigen−antibody binding and MIP, this electrochemical aptasensor demonstrated excellent performance in terms of reproducibility, stability, response time, and high selectivity against other cardiac proteins.

4. MATERIALS AND METHODS

4.1. Chemicals and Materials. Graphite (282863), H_2SO_4 (339741), $KMnO_4$ (223468), H_2O_2 (216763), HCl (H1758), $NaNO_3$ (S5506), $C_2H_3O_2Cl$ (C19627), EDC (3449), BSA (A2153), and myoglobin (Mb; M0630) were procured from Sigma-Aldrich (USA); PEI (P3143) was purchased from Polyscience, Inc, (USA); glass wafers (6 in., Pyrex 7740) were procured from Inexus, Inc., (South Korea); Ag/AgCl ink (RD66) was purchased from BAS Inc. (Tokyo, Japan); Mb aptamer (089) was obtained from OTC Biotech (USA), and its sequence was 5′-ATCCGTCA-CACCTGCTCTTAATTACAGGCAGTTCCACTTAGA-CAG ACACACGAATGGTGTTGGCTCCCGTAT-3; cTnT (9202-1107) and cTnI (9202-0707) antigens were purchased

https://dx.doi.org/10.1021/acsomega.9b03368
ACS Omega 2020, 5, 3924−3931

from AbD Serotec (USA); normal human serum (S1-100ML) was procured from Merck Millipore (USA); NaOH (S1011) and diethylpyrocarbonate (DEPC)-treated water (W2004) were obtained from Biosesang (South Korea); and PBS (pH 7.4, 10×) was procured from Life Technologies (South Korea) and 10-fold-diluted. DEPC-treated water was used for dilution of the aptamer stock solution, which was stored at −20 °C before use.

4.2. Instruments. Raman spectroscopy (300R, WITec, Germany) and FTIR−ATR (VARIAN 670/620, CA, USA) were used to characterize the GO and PEI−rGO thin film. UV−vis spectra were recorded using a liquid spectrophotometer (UV−vis−NIR; Cary 5000, Agilent, USA). A field-emission scanning electron microscope (S-4800, Hitachi, Japan) was used to image the PEI−rGO thin films on ITO/glass electrodes. The samples were coated with platinum by ion sputtering (E-1045, Hitachi, Japan). The chemical bonding of the synthesized GO and PEI−rGO thin films was studied by XPS (K-Alpha, Thermo Scientific, USA). The synthesized GO and PEI−rGO sheets were also characterized using a tapping mode atomic force microscope (Bruker Instrument, USA). All electrochemical measurements were recorded using an Autolab System (PGSTAT204, Metrohm, Netherlands) controlled by the NOVA 1.10 software at room temperature (23 ± 2 °C). All the measurements (otherwise mentioned) were performed in 5 mM $[Fe(CN)_6]^{3-/4-}$ and 0.5 M KCl (1× PBS, pH 7.4) with a three-electrode system comprising a working electrode (ITO/glass; [2 cm × 0.5]), a reference electrode (Ag/AgCl), and a counter electrode (Pt).

4.3. Synthesis of GO and PEI−rGO. GO was synthesized using the modified Hummer's method,[45,59] and its detailed process was previously reported.[60] The GO suspension was treated with EDC (10 mM) with 60 min of sonication and with PEI solution (500 $\mu g\ mL^{-1}$). The resulting solution was kept reacting overnight at room temperature. PEI was covalently attached via binding of $-NH_2$ groups of PEI with −COOH-modified GO using EDC chemistry. The color of GO solution (dark brown) changed from dark brown to black, implying the reduction of GO. The resulting solution (PEI−rGO) was washed with deionized (DI) water three times and centrifuged at 5000 rpm (83 s^{-1}) to remove unbounded PEI and organic impurities. An aqueous solution of the PEI−rGO matrix was prepared by sonicating for 30 min to remove any aggregates, centrifuging the solution at 5000 rpm (83 s^{-1}) for 30 min, and then collecting the supernatant. The PEI−rGO aqueous suspension was very stable, and no distinct precipitate was observed even after several weeks of storage. Figure S1 shows the mechanism of −COOH-modified GO and synthesis of the PEI−rGO matrix.

4.4. Fabrication of the ITO/Glass Electrode. A piranha solution (H_2SO_4/H_2O_2 = 3:1) was used to clean the glass wafer (6 in.) for 10 min, and the wafer was rinsed with DI water and dried with nitrogen (N_2) gas. Indium tin oxide (ITO) (thickness: 100 nm) was deposited by RF-sputtering on the glass wafer and annealed at 400 °C for 1 h. The ITO-coated glass wafer was diced into strips (2 cm × 0.5 cm) acting as working electrodes; cleaned with acetone, methanol, and DI water; and dried with N_2 gas. The electrode was incubated in a solution composed of H_2O, NH_4OH, and H_2O_2 [5:1:1 (v/v)] at 60 °C for 30 min in an oven for hydrolysis, and the solution was quickly quenched with DI water for 2 min. Subsequently, the electrodes were washed with DI water several times and dried with N_2 gas.

4.5. Biofunctionalization of the PEI−rGO-Modified ITO/Glass Electrode. As prepared, PEI−rGO aqueous suspension (10 μL) was drop-cast onto the cleaned ITO/glass electrodes, which were then dried at 60 °C in an oven for 1 h. A homogeneous and thin film of PEI−rGO was formed on the ITO/glass electrodes, rinsed with DI water, and dried with N_2 gas. Afterward, the PEI−rGO thin film-coated ITO/glass electrode was incubated with DNA Mb aptamers (concentration: 12 $\mu g\ mL^{-1}$) in DEPC-treated water at 37 °C for 2 h, thoroughly rinsed with PBS to remove loosely attached aptamers, and air-dried at room temperature for 5 min. The negatively charged Mb aptamers were attached to positively charged PEI−rGO surfaces. The PEI−rGO-coated ITO/glass electrodes were then incubated with BSA (1mg mL^{-1}) at room temperature for 30 min to preclude possible nonspecific binding and rinsed with PBS. The electrochemical measurements were performed for Mb (0.001−1000 ng mL^{-1}) in PBS and human serum (10-fold-diluted) in PBS.

■ ASSOCIATED CONTENT

Supporting Information

The Supporting Information is available free of charge at https://pubs.acs.org/doi/10.1021/acsomega.9b03368.

More characterization techniques (HR-TEM, UV−vis, and Raman spectra) to verify the formation of PEI-rGO; optimization of aptamer concentrations and binding time of aptamer/antigen; scan rate effects; EIS parameters at different stages of immobilizations; and RSD values of the reproducibility assay (PDF)

■ AUTHOR INFORMATION

Corresponding Author

Jaesung Jang − *Department of Biomedical Engineering and School of Mechanical, Aerospace and Nuclear Engineering, UNIST, Ulsan 44919, Republic of Korea;* orcid.org/0000-0002-7833-6925; Phone: +82-52-217-2323; Email: jjang@unist.ac.kr; Fax: +82-52-217-2449

Authors

Abhinav Sharma − *School of Materials Science and Engineering, Ulsan National Institute of Science and Technology (UNIST), Ulsan 44919, Republic of Korea*

Jyoti Bhardwaj − *Department of Biomedical Engineering, UNIST, Ulsan 44919, Republic of Korea*

Complete contact information is available at: https://pubs.acs.org/10.1021/acsomega.9b03368

Author Contributions

‖A.S. and J.B. contributed equally to this work.

Notes

The authors declare no competing financial interest.

■ ACKNOWLEDGMENTS

This research was supported by the 2019 Research Fund (1.190011.01) of UNIST, by the MSIT (Ministry of Science and ICT), Korea, under the ITRC (Information Technology Research Center) support program (IITP-2018-2017-0-01635) supervised by the IITP (Institute for Information & communications Technology Promotion), and by the National Research Foundation of Korea (NRF) grant funded by the Korea government (MSIT) (no. 2019R1H1A2039725). The authors would also like to acknowledge and thank the staff in

https://dx.doi.org/10.1021/acsomega.9b03368
ACS Omega 2020, 5, 3924−3931

the UNIST Central Research Facilities (UCRF) for their help in this study.

REFERENCES

(1) McDonnell, B.; Hearty, S.; Leonard, P.; O'Kennedy, R. Cardiac Biomarkers and the Case for Point-of-Care Testing. *Clin. Biochem.* **2009**, *42*, 549−561.
(2) Suprun, E.; Bulko, T.; Lisitsa, A.; Gnedenko, O.; Ivanov, A.; Shumyantseva, V.; Archakov, A. Electrochemical Nanobiosensor for Express Diagnosis of Acute Myocardial Infarction in Undiluted Plasma. *Biosens. Bioelectron.* **2010**, *25*, 1694−1698.
(3) Friess, U.; Stark, M. Cardiac Markers: A Clear Cause for Point-of-Care Testing. *Anal. Bioanal. Chem.* **2009**, *393*, 1453−1462.
(4) Mohammed, M.-I.; Desmulliez, M. P. Y. Lab-on-a-Chip Based Immunosensor Principles and Technologies for the Detection of Cardiac Biomarkers: A Review. *Lab Chip* **2011**, *11*, 569−595.
(5) Tuteja, S. K.; Chen, R.; Kukkar, M.; Song, C. K.; Mutreja, R.; Singh, S.; Paul, A. K.; Lee, H.; Kim, K.-H.; Deep, A.; Suri, C. R. A Label-Free Electrochemical Immunosensor for the Detection of Cardiac Marker Using Graphene Quantum Dots (GQDs). *Biosens. Bioelectron.* **2016**, *86*, 548−556.
(6) Naveena, B. M.; Faustman, C.; Tatiyaborworntham, N.; Yin, S.; Ramanathan, R.; Mancini, R. A. Detection of 4-Hydroxy-2-Nonenal Adducts of Turkey and Chicken Myoglobins Using Mass Spectrometry. *Food Chem.* **2010**, *122*, 836−840.
(7) Giaretta, N.; Di Giuseppe, A. M. A.; Lippert, M.; Parente, A.; Di Maro, A. Myoglobin as Marker in Meat Adulteration: A UPLC Method for Determining the Presence of Pork Meat in Raw Beef Burger. *Food Chem.* **2013**, *141*, 1814−1820.
(8) Gnedenko, O. V.; Mezentsev, Y. V.; Molnar, A. A.; Lisitsa, A. V.; Ivanov, A. S.; Archakov, A. I. Highly Sensitive Detection of Human Cardiac Myoglobin Using a Reverse Sandwich Immunoassay with a Gold Nanoparticle-Enhanced Surface Plasmon Resonance Biosensor. *Anal. Chim. Acta* **2013**, *759*, 105−109.
(9) Osman, B.; Uzun, L.; Beşirli, N.; Denizli, A. Microcontact Imprinted Surface Plasmon Resonance Sensor for Myoglobin Detection. *Mater. Sci. Eng. C* **2013**, *33*, 3609−3614.
(10) Wang, Q.; Yang, X.; Liu, F.; Wang, K. Visual Detection of Myoglobin via G-Quadruplex DNAzyme Functionalized Gold Nanoparticles-Based Colorimetric Biosensor. *Sensors Actuators B Chem* **2015**, *212*, 440−445.
(11) Chen, J.; Ran, F.; Chen, Q.; Luo, D.; Ma, W.; Han, T.; Wang, C.; Wang, C. A fluorescent biosensor for cardiac biomarker myoglobin detection based on carbon dots and deoxyribonuclease I-aided target recycling signal amplification. *RSC Adv.* **2019**, *9*, 4463−4468.
(12) Lee, I.; Luo, X.; Cui, X. T.; Yun, M. Highly Sensitive Single Polyaniline Nanowire Biosensor for the Detection of Immunoglobulin G and Myoglobin. *Biosens. Bioelectron.* **2011**, *26*, 3297−3302.
(13) Shumyantseva, V. V.; Bulko, T. V.; Sigolaeva, L. V.; Kuzikov, A. V.; Shatskaya, M. A.; Archakov, A. I. Electrosynthesis and Binding Properties of Molecularly Imprinted Poly-o-Phenylenediamine as Artificial Antibodies for Electroanalysis of Myoglobin. *Dokl. Biochem. Biophys.* **2015**, *464*, 275−278.
(14) Moreira, F. T. C.; Dutra, R. A. F.; Noronha, J. P. C.; Sales, M. G. F. Electrochemical Biosensor Based on Biomimetic Material for Myoglobin Detection. *Electrochim. Acta* **2013**, *107*, 481−487.
(15) Ribeiro, J. A.; Pereira, C. M.; Silva, A. F.; Sales, M. G. F. Electrochemical Detection of Cardiac Biomarker Myoglobin Using Polyphenol as Imprinted Polymer Receptor. *Anal. Chim. Acta* **2017**, *981*, 41−52.
(16) Menger, M.; Yarman, A.; Erdőssy, J.; Yildiz, H.; Gyurcsányi, R.; Scheller, F. MIPs and Aptamers for Recognition of Proteins in Biomimetic Sensing. *Biosensors* **2016**, *6* . DOI: DOI: 10.3390/bios6030035.
(17) Srivastava, M.; Nirala, N. R.; Srivastava, S. K.; Prakash, R. A Comparative Study of Aptasensor vs Immunosensor for Label-Free PSA Cancer Detection on GQDs-AuNRs Modified Screen-Printed Electrodes. *Sci. Rep.* **2018**, *8*, 1923.
(18) Taghdisi, S. M.; Danesh, N. M.; Ramezani, M.; Emrani, A. S.; Abnous, K. A Novel Electrochemical Aptasensor Based on Y-Shape Structure of Dual-Aptamer-Complementary Strand Conjugate for Ultrasensitive Detection of Myoglobin. *Biosens. Bioelectron.* **2016**, *80*, 532−537.
(19) Dai, Z.; Xiao, Y.; Yu, X.; Mai, Z.; Zhao, X.; Zou, X. Direct Electrochemistry of Myoglobin Based on Ionic Liquid-Clay Composite Films. *Biosens. Bioelectron.* **2009**, *24*, 1629−1634.
(20) Bai, H.-Y.; Campo, F. J. D.; Tsai, Y.-C.; Tsai, Y.-C. Sensitive Electrochemical Thrombin Aptasensor Based on Gold Disk Microelectrode Arrays. *Biosens. Bioelectron.* **2013**, *42*, 17−22.
(21) Wang, Z.; Dai, Z. Carbon Nanomaterial-Based Electrochemical Biosensors: An Overview. *Nanoscale* **2015**, *7*, 6420−6431.
(22) Geim, A. K.; Novoselov, K. S. The Rise of Graphene. *Nat. Mater.* **2007**, *6*, 183−191.
(23) Huang, X.; Zeng, Z.; Fan, Z.; Liu, J.; Zhang, H. Graphene-Based Electrodes. *Adv. Mater.* **2012**, *24*, 5979−6004.
(24) Stankovich, S.; Dikin, D. A.; Piner, R. D.; Kohlhaas, K. A.; Kleinhammes, A.; Jia, Y.; Wu, Y.; Nguyen, S. T.; Ruoff, R. S. Synthesis of Graphene-Based Nanosheets via Chemical Reduction of Exfoliated Graphite Oxide. *Carbon* **2007**, *45*, 1558−1565.
(25) Stankovich, S.; Dikin, D. A.; Dommett, G. H. B.; Kohlhaas, K. M.; Zimney, E. J.; Stach, E. A.; Piner, R. D.; Nguyen, S. T.; Ruoff, R. S. Graphene-Based Composite Materials. *Nature* **2006**, *442*, 282−286.
(26) Shin, H. J.; Kim, K. K.; Benayad, A.; Yoon, S. M.; Park, H. K.; Jung, I. S.; Jin, M. H.; Jeong, H. K.; Kim, J. M.; Choi, J. Y.; Lee, Y. H. Efficient Reduction of Graphite Oxide by Sodium Borohydride and Its Effect on Electrical Conductance. *Adv. Funct. Mater.* **2009**, *19*, 1987−1992.
(27) Feng, X.-M.; Li, R.-M.; Ma, Y.-W.; Chen, R.-F.; Shi, N.-E.; Fan, Q.-L.; Huang, W. One-Step Electrochemical Synthesis of Graphene/Polyaniline Composite Film and Its Applications. *Adv. Funct. Mater.* **2011**, *21*, 2989−2996.
(28) Alwarappan, S.; Liu, C.; Kumar, A.; Li, C.-Z. Enzyme-Doped Graphene Nanosheets for Enhanced Glucose Biosensing. *J. Phys. Chem. C* **2010**, *114*, 12920−12924.
(29) Zhang, Z.; Liu, S.; Shi, Y.; Zhang, Y.; Peacock, D.; Yan, F.; Wang, P.; He, L.; Feng, X.; Fang, S. Label-Free Aptamer Biosensor for Thrombin Detection on a Nanocomposite of Graphene and Plasma Polymerized Allylamine. *J. Mater. Chem. B* **2014**, *2*, 1530−1538.
(30) Su, X.; Ren, J.; Meng, X.; Ren, X.; Tang, F. A Novel Platform for Enhanced Biosensing Based on the Synergy Effects of Electrospun Polymer Nanofibers and Graphene Oxides. *Analyst* **2013**, *138*, 1459−1466.
(31) Jia, L.; Liu, J.; Wang, H. Preparation of Poly-(Diallyldimethylammonium Chloride)-Functionalized Graphene and Its Applications for H_2O_2 and Glucose Sensing. *Electrochim. Acta* **2013**, *111*, 411−418.
(32) Feng, L.; Zhang, S.; Liu, Z. Graphene Based Gene Transfection. *Nanoscale* **2011**, *3*, 1252.
(33) Chen, B.; Liu, M.; Zhang, L.; Huang, J.; Yao, J.; Zhang, Z.; Gorchinskiy, A. D.; Liu, J.; Lin, Y. H. Polyethylenimine-Functionalized Graphene Oxide as an Efficient Gene Delivery Vector. *J. Mater. Chem.* **2011**, *21*, 7736−7741.
(34) Shan, C.; Wang, L.; Han, D.; Li, F.; Zhang, Q.; Zhang, X.; Niu, L. Polyethyleneimine-Functionalized Graphene and Its Layer-by-Layer Assembly with Prussian Blue. *Thin Solid Films* **2013**, *534*, 572−576.
(35) Xu, C.; Zhang, L.; Liu, L.; Shi, Y.; Wang, H.; Wang, X.; Wang, F.; Yuan, B.; Zhang, D. A Novel Enzyme-Free Hydrogen Peroxide Sensor Based on Polyethylenimine-Grafted Graphene Oxide-Pd Particles Modified Electrode. *J. Electroanal. Chem.* **2014**, *731*, 67−71.
(36) Kahlouche, K.; Jijie, R.; Hosu, I.; Barras, A.; Gharbi, T.; Yahiaoui, R.; Herlem, G.; Ferhat, M.; Szunerits, S.; Boukherroub, R. Controlled modification of electrochemical microsystems with polyethylenimine/reduced graphene oxide using electrophoretic deposition: Sensing of dopamine levels in meat samples. *Talanta* **2018**, *178*, 432−440.

https://dx.doi.org/10.1021/acsomega.9b03368
ACS Omega 2020, 5, 3924−3931

(37) Ponnusamy, V. K.; Mani, V.; Chen, S.-M.; Huang, W.-T. Talanta Rapid Microwave Assisted Synthesis of Graphene Nanosheets/Polyethyleneimine/Gold Nanoparticle Composite and Its Application to the Selective Electrochemical Determination of Dopamine. *Talanta* **2014**, *120*, 148−157.
(38) Jijie, R.; Kahlouche, K.; Barras, A.; Yamakawa, N.; Bouckaert, J.; Gharbi, T.; Szunerits, S.; Boukherroub, R. Reduced graphene oxide/polyethylenimine based immunosensor for the selective and sensitive electrochemical detection of uropathogenic Escherichia coli. *Sensors Actuators B. Chem.* **2018**, *260*, 255−263.
(39) Hemanth, S.; Halder, A.; Caviglia, C.; Chi, Q.; Keller, S. 3D Carbon Microelectrodes with Bio-Functionalized Graphene for Electrochemical Biosensing. *Biosensors* **2018**, *8*, 70−79.
(40) Luo, J. H.; Li, B. L.; Li, N. B.; Luo, H. Q. Sensitive detection of gallic acid based on polyethyleneimine-functionalized graphene modified glassy carbon electrode. *Sensors Actuators B. Chem.* **2013**, *186*, 84−89.
(41) Hu, R.; Gou, H.; Mo, Z.; Wei, X.; Wang, Y. Highly Selective Detection of Trace Cu^{2+} Based on Polyethyleneimine-Reduced Graphene Oxide Nanocomposite Modified Glassy Carbon Electrode. *Ionics* **2015**, *21*, 3125−3133.
(42) Song, M.; Xu, J. Preparation of Polyethylenimine-Functionalized Graphene Oxide Composite and Its Application in Electrochemical Ammonia Sensors. *Electroanalysis* **2013**, *25*, 523−530.
(43) Cui, D.; Mi, L.; Xu, X.; Lu, J.; Qian, J.; Liu, S. Nanocomposites of Graphene and Cytochrome P450 2D6 Isozyme for Electrochemical-Driven Tramadol Metabolism. *Langmuir* **2014**, *30*, 11833−11840.
(44) Grabowska, I.; Sharma, N.; Vasilescu, A.; Iancu, M.; Badea, G.; Boukherroub, R.; Ogale, S.; Szunerits, S. Electrochemical Aptamer-Based Biosensors for the Detection of Cardiac Biomarkers. *ACS Omega* **2018**, *3*, 12010−12018.
(45) Hummers, W. S.; Offeman, R. E. Preparation of Graphitic Oxide. *J. Am. Chem. Soc.* **1958**, *80*, 1339.
(46) Zhao, C.; Xing, L.; Xiang, J.; Cui, L.; Jiao, J.; Sai, H.; Li, Z.; Li, F. Formation of Uniform Reduced Graphene Oxide Films on Modified PET Substrates Using Drop-Casting Method. *Particuology* **2014**, *17*, 66−73.
(47) Gong, P.; Shi, B.; Zheng, M.; Wang, B.; Zhang, P.; Hu, D.; Gao, D.; Sheng, Z.; Zheng, C.; Ma, Y.; Cai, L. PEI Protected Aptamer Molecular Probes for Contrast-Enhanced in Vivo Cancer Imaging. *Biomaterials* **2012**, *33*, 7810−7817.
(48) Stankovich, S.; Piner, R. D.; Chen, X.; Wu, N.; Nguyen, S. T.; Ruoff, R. S.; Talmon, Y. Stable Aqueous Dispersions of Graphitic Nanoplatelets via the Reduction of Exfoliated Graphite Oxide in the Presence of Poly(Sodium 4-Styrenesulfonate). *J. Mater. Chem.* **2006**, *16*, 155−158.
(49) Huang, H.; Lü, S.; Zhang, X.; Shao, Z. Glucono-*δ*-lactone controlled assembly of graphene oxide hydrogels with selectively reversible gel-sol transition. *Soft Matter* **2012**, *8*, 4609−4615.
(50) Hontoria-Lucas, C.; López-Peinado, A. J.; López-González, J. d. D.; Rojas-Cervantes, M. L.; Martín-Aranda, R. M. Study of Oxygen-Containing Groups in a Series of Graphite Oxides: Physical and Chemical Characterization. *Carbon* **1995**, *33*, 1585−1592.
(51) Guo, H.-L.; Wang, X.-F.; Qian, Q.-Y.; Wang, F.-B.; Xia, X.-H. A Green Approach to the Synthesis of Graphene Nanosheets. *ACS Nano* **2009**, *3*, 2653−2659.
(52) Ramanathan, T.; Fisher, F. T.; Ruoff, R. S.; Brinson, L. C. Amino-Functionalized Carbon Nanotubes for Binding to Polymers and Biological Systems. *Chem. Mater.* **2005**, *17*, 1290−1295.
(53) Wu, H.; Huang, D.; Jin, X.; Luo, C.; Dong, Q.; Sun, B.; Zong, R.; Li, J.; Zhang, L.; Zhang, H. Silver Nanoparticles/Polyethyleneimine/Graphene Oxide Composite Combined with Surfactant Film for Construction of an Electrochemical Biosensor. *Anal. Methods* **2016**, *8*, 2961−2966.
(54) Jiao, T.; Guo, H.; Zhang, Q.; Peng, Q.; Tang, Y.; Yan, X.; Li, B. Reduced Graphene Oxide-Based Silver Nanoparticle-Containing Composite Hydrogel as Highly Efficient Dye Catalysts for Wastewater Treatment. *Sci. Rep.* **2015**, *5*, 11873.
(55) Zhang, B.; Zhang, Y.; Liang, W.; Cui, B.; Li, J.; Yu, X.; Huang, L. Nanogold-Penetrated Poly(Amidoamine) Dendrimer for Enzyme-Free Electrochemical Immunoassay of Cardiac Biomarker Using Cathodic Stripping Voltammetric Method. *Anal. Chim. Acta* **2016**, *904*, 51−57.
(56) Sharma, A.; Han, C.-H.; Jang, J. Rapid Electrical Immunoassay of the Cardiac Biomarker Troponin I through Dielectrophoretic Concentration Using Imbedded Electrodes. *Biosens. Bioelectron.* **2016**, *82*, 78−84.
(57) McCann, C. J.; Glover, B. M.; Menown, I. B. A.; Moore, M. J.; McEneny, J.; Owens, C. G.; Smith, B.; Sharpe, P. C.; Young, I. S.; Adgey, J. A. Novel Biomarkers in Early Diagnosis of Acute Myocardial Infarction Compared with Cardiac Troponin T. *Eur. Heart J.* **2008**, *29*, 2843−2850.
(58) Lewandrowski, K.; Adchean, C.; Januzzi, J. Cardiac Markers for Myocardial Infarction. *Am. Soc. Clin. Pathol.* **2002**, *118*, S93−S99.
(59) Park, S.; An, J.; Piner, R. D.; Jung, I.; Yang, D.; Velamakanni, A.; Nguyen, S. T.; Ruoff, R. S. Aqueous Suspension and Characterization of Chemically Modified Graphene Sheets. *Chem. Mater.* **2008**, *20*, 6592−6594.
(60) Sharma, A.; Jang, J. Flexible Electrical Aptasensor Using Dielectrophoretic Assembly of Graphene Oxide and Its Subsequent Reduction for Cardiac Biomarker Detection. *Sci. Rep.* **2019**, *9*, 5970−5980.
(61) Wang, X.; You, Z.; Sha, H.; Sun, Z.; Sun, W. Electrochemical Myoglobin Biosensor Based on Carbon Ionic Liquid Electrode Modified with Fe_3O_4@SiO_2 Microsphere. *J. Solid State Electrochem.* **2014**, *18*, 207−213.
(62) Pakapongpan, S.; Palangsuntikul, R.; Surareungchai, W. Electrochemical Sensors for Hemoglobin and Myoglobin Detection Based on Methylene Blue-Multiwalled Carbon Nanotubes Nanohybrid-Modified Glassy Carbon Electrode. *Electrochim. Acta* **2011**, *56*, 6831−6836.
(63) Li, C.; Li, J.; Yang, X.; Gao, L.; Jing, L.; Ma, X. A Label-Free Electrochemical Aptasensor for Sensitive Myoglobin Detection in Meat. *Sensors Actuators B. Chem.* **2017**, *242*, 1239−1245.
(64) Rajesh; Sharma, V.; Tanwar, V. K.; Mishra, S. K.; Biradar, A. M. Electrochemical Impedance Immunosensor for the Detection of Cardiac Biomarker Myogobin (Mb) in Aqueous Solution. *Thin Solid Films* **2010**, *519*, 1167−1170.
(65) Singh, S.; Tuteja, S. K.; Sillu, D.; Deep, A.; Suri, C. R. Gold Nanoparticles-Reduced Graphene Oxide Based Electrochemical Immunosensor for the Cardiac Biomarker Myoglobin. *Microchim. Acta* **2016**, *183*, 1729−1738.
(66) Kumar, V.; Shorie, M.; Ganguli, A. K.; Sabherwal, P. Graphene-CNT Nanohybrid Aptasensor for Label Free Detection of Cardiac Biomarker Myoglobin. *Biosens. Bioelectron.* **2015**, *72*, 56−60.
(67) Suprun, E.; Bulko, T.; Lisitsa, A.; Gnedenko, O.; Ivanov, A.; Shumyantseva, V.; Archakov, A. Electrochemical Nanobiosensor for Express Diagnosis of Acute Myocardial Infarction in Undiluted Plasma. *Biosens. Bioelectron.* **2010**, *25*, 1694−1698.
(68) Mishra, S. K.; Srivastava, A. K.; Kumar, D.; Rajesh, R. Bio-Functionalized Pt Nanoparticles Based Electrochemical Impedance Immunosensor for Human Cardiac Myoglobin. *RSC Adv.* **2014**, *4*, 21267−21276.
(69) Ren, X.; Zhang, Y.; Sun, Y.; Gao, L. Development of Electrochemical Impedance Immunosensor for Sensitive Determination of Myoglobin. *Int. J. Electrochem. Sci.* **2017**, *12*, 7765−7776.
(70) Zhang, G.; Liu, Z.; Wang, L.; Guo, Y. Electrochemical Aptasensor for Myoglobin-Specific Recognition Based on Porphyrin Functionalized Graphene-Conjugated Gold Nanocomposites. *Sensors* **2016**, *16*, 1803−1815.
(71) Khan, R.; Pal, M.; Kuzikov, A. V.; Bulko, T.; Suprun, E. V.; Shumyantseva, V. V. Impedimetric Immunosensor for Detection of Cardiovascular Disorder Risk Biomarker. *Mater. Sci. Eng. C* **2016**, *68*, 52−58.

https://dx.doi.org/10.1021/acsomega.9b03368
ACS Omega 2020, 5, 3924−3931